THE ASTROPHYSICAL JOURNAL, 426:553–562, 1994 May 10

UIT: ULTRAVIOLET SURFACE PHOTOMETRY OF THE SPIRAL GALAXY M74 (NGC 628)

ROBERT H. CORNETT,[1] ROBERT W. O'CONNELL,[2] MICHAEL R. GREASON,[1] JOEL D. OFFENBERG,[1]
RONALD J. ANGIONE,[3] RALPH C. BOHLIN,[4] K. P. CHENG,[5] MORTON S. ROBERTS,[6]
ANDREW M. SMITH,[5] ERIC P. SMITH,[5] FRED D. TALBERT,[3] AND THEODORE P. STECHER[5]
Received 1993 September 17; accepted 1993 November 16

ABSTRACT

Ultraviolet photometry, obtained from Ultraviolet Imaging Telescope (UIT) images at 1520 Å [far-UV; magnitudes $m(152)$] and 2490 Å [near-UV; magnitudes $m(249)$], of the spiral galaxy M74 (NGC 628) is compared with Hα, R, V, and B surface photometry and with models. M74's surface brightness profiles have a central peak with an exponential falloff; the exponential scale lengths of the profiles increase with decreasing wavelength for the broad-band images. The slope of the continuum-subtracted Hα profile is intermediate between those of far-UV and near-UV profiles, consistent with the related origins of $H\alpha$ and UV emission in extreme Population I material.

M74's color profiles all become bluer with increasing radius. The $[m(152) - m(249)]$ color as measured by UIT averages near 0.0 (the color of an A0 star) over the central 20″ radius and decreases from ~ -0.2 to ~ -0.4 from 20″ to 200″. The spiral arms are the dominant component of the surface photometry colors; interarm regions are slightly redder. In the UV, M74's nuclear region resembles its disk/spiral arm material in colors and morphology, unlike galaxies such as M81. No UV "bulge" is apparent. The $m(152) - m(249)$ colors and models of M74's central region clearly demonstrate that there is no significant population of O or B stars present in the central 10″.

M74's UV morphology and $[m(152) - m(249)]$ color profiles are similar to those of M33, although M74 is $\sim$0.5 mag redder. M81 has a smooth UV bulge which is much redder than the nuclear regions of M74 and M33. M74 is $\sim$0.4 mag bluer than M81 in its outer disk, although M81 has bright UV sources only in spiral arms more than 5 kpc from its center. We investigate possible explanations for the color profiles of the galaxies and the differences among the galaxies: abundances; reddening due to internal dust; IMF variations, and the history of formation of the dominant generations of stars. Abundance and IMF variations do not produce large enough $m(152) - m(249)$ or UV $- V$ color differences.

Comparing model UV/optical colors with those of M74 shows that M74's disk has undergone significant star formation over the past 500 Myr, and that either the star-formation history or the extinction varies systematically across M74's disk. Realistic reddening models show that the effects of dust alone are not sufficient to produce the variations within M74. However, evolutionary models produced by combining data from stellar atmosphere models and observed spectra generate UV $- V$ colors which are compatible with the observations, provided relatively recent star formation is present in the stellar population.

Comparison of M74, M33, and M81 (UV $- V$) colors shows that M74 colors range from the bluest of M33's colors to the bluest of M81's. All material with these colors in all three galaxies has the morphological appearance of spiral arm/disk material. The failure of reddening models to cover the range of colors, and the known abundance range in such material, leads to the conclusion that star-formation history varies significantly as a function of radius in these galaxies, and that such variation is required to explain the range of colors observed in M74, M33, and M81.

Subject headings: galaxies: individual (NGC 628) — galaxies: photometry — galaxies: spiral — ultraviolet: galaxies

1. INTRODUCTION

M74 (NGC 628) is an ScI galaxy with a Holmberg radius of 6′, which is viewed nearly face-on with an inclination angle of 5°–7° (Shostak & van der Kruit 1984). It represents a good opportunity for photometric studies that are relatively unaffected by differential effects of internal dust. We obtained vacuum ultraviolet images of M74 with the Ultraviolet Imaging Telescope (UIT) during the Astro-1 mission in 1990 December. Preliminary discussions of these observations, with emphasis on spiral morphology, were presented by Chen et al. (1992). Here, we present results of large-scale surface photometry in far-UV (FUV), near-UV (NUV), B, V, R, and Hα bandpasses.

[1] Hughes STX Corporation, Code 681, Goddard Space Flight Center, Greenbelt MD 20771.
[2] University of Virginia, Astronomy Department, P.O. Box 3818, Charlottesville, VA 22903.
[3] San Diego State University, Astronomy Department, San Diego, CA 92182-0540.
[4] Space Telescope Science Institute, Homewood Campus, Baltimore, MD 21218.
[5] Laboratory for Astronomy and Solar Physics, Code 680, Goddard Space Flight Center, Greenbelt MD 20771.
[6] National Radio Astronomy Observatory, Edgemont Road, Charlottesville, VA 22903.

2. OBSERVATIONAL DATA

2.1. *UIT Observations*

M74 was observed by UIT on two orbits on 1990 December 6. UIT is a 38 cm diameter f/9 Ritchey-Chretien telescope employing two magnetically focused ITT image intensifiers

coupled to Kodak IIa-O film; a description of UIT and its calibration, operation, and standard reduction procedures is in Stecher et al. (1992). Ten UIT exposures, with 40 arcmin diameter fields of view, were made of M74 in various filter/camera combinations. The two longest exposures, one each in the NUV and FUV cameras, were measured and analysed for the present discussion. The NUV image is UIT frame NUV0161, has exposure time 560 s, and was made with filter A1, which has an effective wavelength $\lambda_{\rm eff}$ for an energy distribution $F_\lambda \sim$ constant of 2490 Å. The FUV image, UIT frame FUV0172, was made with filter B1 and has exposure time 600 s and $\lambda_{\rm eff} = 1520$ Å. A part of the NUV image is shown in Figure 1, with our ground-based V-band image displayed with the same scale and orientation. North is up and east is left. Magnitudes derived from the A1 and B1 filters are called $m(249)$ and $m(152)$, respectively, and are defined by $m = -2.5 \log (F_\lambda) - 21.1$, where the units of F_λ are ergs cm^{-2} Å^{-1} s^{-1}.

For the present paper, the original UIT images were digitized with the usual 20 μm pixels but with a 10 μm separation, which is half the usual spacing. The pixel separation is 0.″57; the full width at half-maximum (FWHM) of a Gaussian fit to stellar images is 2.″7, which includes the effects of the finite digitization aperture. Standard UIT data reduction uses digitization with 20 μm pixels and 20 μm separation, with a corresponding pixel size of 1.″14 on the sky and a FWHM for stellar images of typically 3″. The standard 20 μm pixel size permits processing and calibrating the images using the same parameters as in Stecher et al. (1992), while oversampling with smaller pixel separation permits improved effective resolution.

Chen et al. (1992) reported the discovery on the UIT images of a blue diffuse object 7.′6 southwest of M74's center. Further analysis of the images has shown this object to be the afterglow of a bright star present on images of an earlier exposure series; it is therefore spurious.

2.2. *Groundbased Observations*

Direct CCD images of the spiral galaxy M74 were obtained in 1991 October from San Diego State University's Mount Laguna Observatory. For these observations, a focal reducer was used in conjunction with a TI 880^2 CCD on a 1 m telescope. Data were obtained using a 50 mm camera lens that yields an 18 arcmin square field of view for each image. With $\sim$2″ seeing, the resolution of the ground-based images closely matches the UIT resolution. Multiple integrations in each filter total 30 minutes in B, 15 minutes in V, 9 minutes in R, and 45 minutes in Hα. Exposures in each passband were median filtered to remove radiation events and maximize the dynamic range. The data were reduced using standard IRAF software; standard stars were observed for the absolute flux calibration. Our B and V magnitudes for M74's nucleus agree with those of de Vaucouleurs, de Vaucouleurs, & Corwin (1978) within 0.05 (1 σ). Subsequent image analysis was carried out using the interactive UIT MOUSSE image processing package developed at Godard Space Flight Center.

Because a pure off-band image was not available, we adopt a procedure similar to that of Belley & Roy (1992) to remove the effects of continuum from the Hα images. This procedure is a compromise between requiring field stars to have nearly zero net flux on the Hα minus scaled-R image and requiring no large-scale variations in the difference image across the nuclear region. The resulting image, which we use as a continuum-subtracted Hα image and call "CSHα," satisfies those criteria and, in addition, has zero net Hα flux from the central 20″ of M74's nuclear region, which is consistent with the observations of Pronik (1973). We calibrate the CSHα data by comparing our measured flux with the results of Kennicutt & Hodge (1980) and obtain a 1 σ uncertainty of 2.4% from the consistency of our measurements of their three H II regions 627, 598, and 292.

TABLE 1

SKY BRIGHTNESS AND UNCERTAINIES

Bandpass	Brightness (mag arcsec^{-2})	σ
FUV	24.34	0.46
NUV	24.81	0.07
B	21.89	0.010
V	20.86	0.008
R	20.28	0.004

3. LARGE-SCALE PHOTOMETRY

3.1. *Annular Surface Photometry*

We have measured the large-scale flux, surface brightness, and color distribution of M74 in circular annular apertures from 2.″3 to 340″ in radius, with annulus widths increasing from 1.″1 in the center to 14″ for the largest annuli. Photometry was derived for the FUV, NUV, B, V, R, Hα, and CSHα images. Sky brightness and its uncertainty were measured by determining the mean flux in approximately 30 18″ × 18″ regions surrounding the galaxy in each image and computing the mean and standard deviation of those values. Results of these measurements for the continuum images are shown in Table 1; the UV sky is 3.5–4.0 mag arcsec^{-2} fainter than in V, according to our definition of UV magnitude in § 2.1. For all images, the 18″ × 18″ aperture size is large enough to reduce the contribution of the pixel-to-pixel noise to insignificance, so that the σ values listed measure the real sky uncertainty. In the UV images this uncertainty is caused by large-scale variations across the frames due to variations in the film as measured by a PDS microdensitometer, since dark frames show similar scatter.

Photometric results in the form of surface brightness plots are presented in Figure 2. M74's surface brightness profile in all bandpasses consists of a nuclear peak about 30″ in radius and an approximately exponential decline out to about 300″ radius, beyond which the data are unreliable due to uncertain sky brightness. The FUV and NUV surface brightness profiles are flatter, i.e., have smaller gradients, than the optical continuum profiles. Table 2 contains scale lengths, derived from linear least-square fits to log-luminosity/radius data, for radii $75'' < R < 300''$, and shows that the scale length of the disk surface brightness in the continuum monotonically decreases with λ. The scale length of the CSHα profile is approximately

TABLE 2

FITS TO SURFACE BRIGHTNESS PROFILES

Bandpass	Scale Length	σ
FUV	121.″7	5.6
NUV	97.9	4.2
B	92.2	7.7
V	83.0	4.5
R	82.1	5.7
CSHα	118.1	18.0

1994ApJ...426..553C

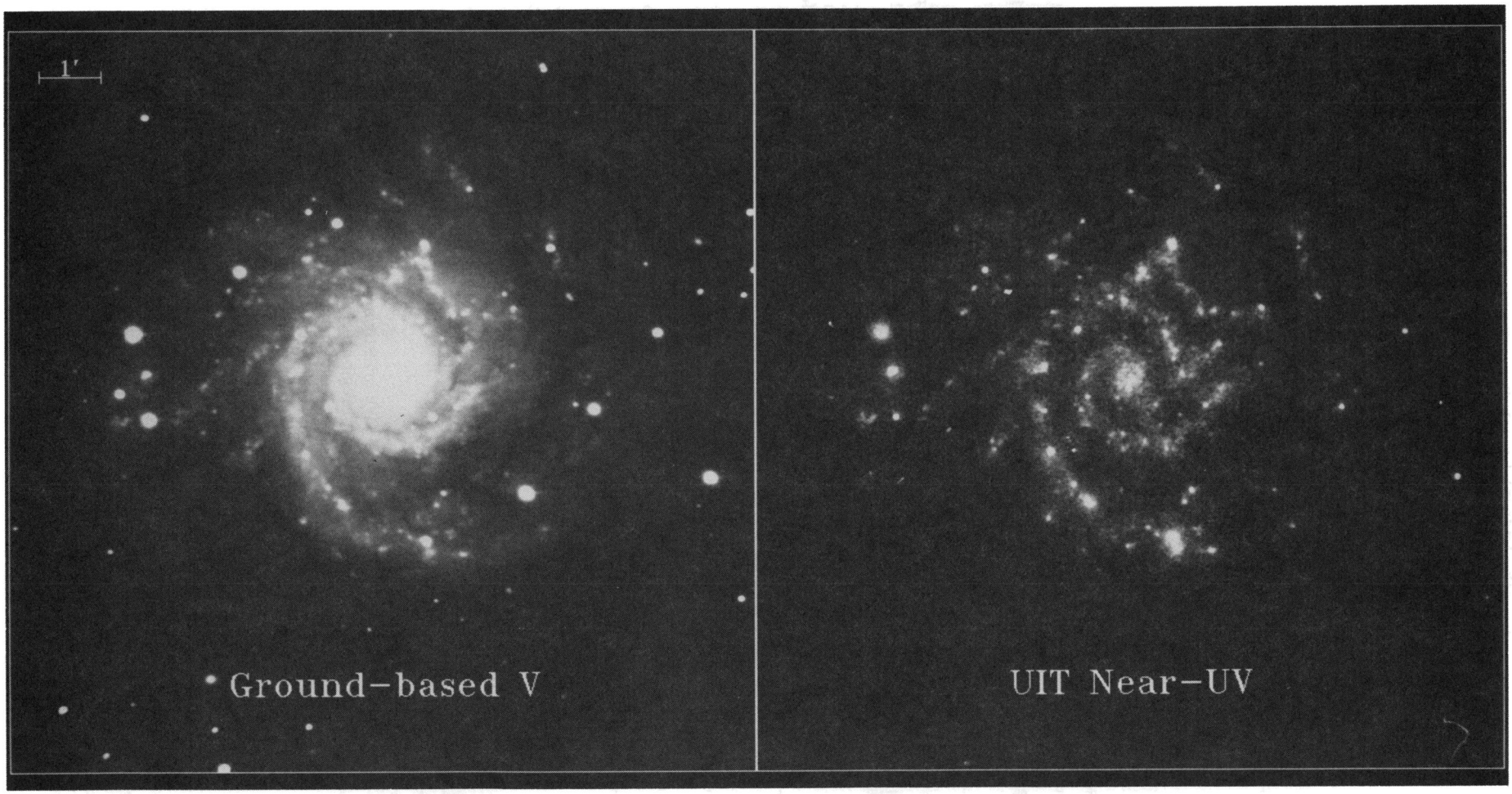

FIG. 1*a*

FIG. 1*b*

FIG. 1.—(*a*) Ground-based *V*-band image of M74. North is up, east is left, and a 1′ bar is marked. (*b*) The UIT NUV image displayed with the same scale and orientation as (*a*). This image was made through the broad-band A1 filter, which has an effective wavelength for flat spectra of 2490 Å. Note the relative strength of the bulge in *V*, its weakness in the NUV, and the apparent NUV uniformity with radius of the disk material in relative brightness and morphology.

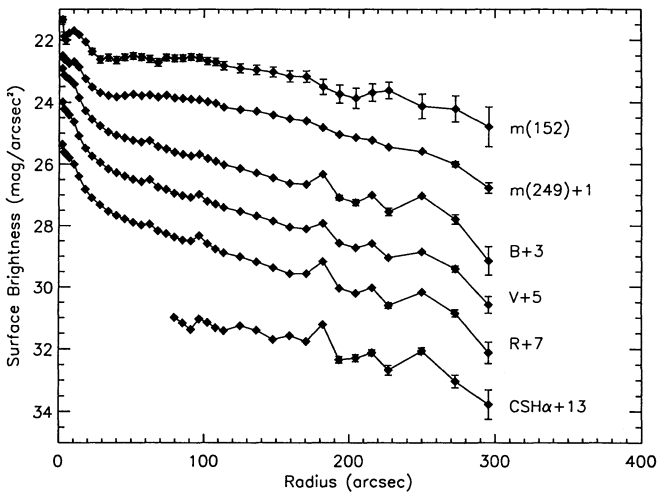

FIG. 2.—Radial surface brightness profiles for M74 in $m(152)$, $m(249)$, B, V, R, and continuum-subtracted Hα (CSHα). The 1 σ error bars are displayed where they are larger than plot symbols. The $m(249)$, B, V, R, and CSHα curves have been shifted vertically by the amounts noted. Surface brightness values for the CSHα profile are uncertain for radii $\leq 75''$ because of uncertainties in the continuum subtraction process and are not plotted.

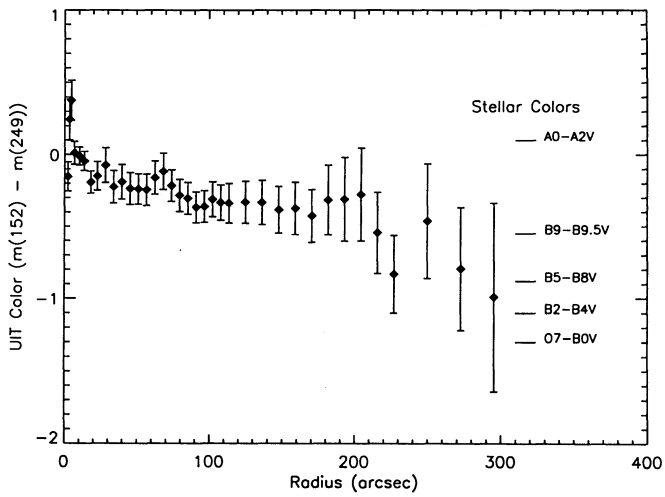

FIG. 4.—Radial UV color [$m(152) - m(249)$] profile for M74. The 1 σ error bars include mean sky, sky noise, and signal uncertainties but not UIT absolute calibration uncertainties. Stellar colors computed from the UV spectral atlas of Fanelli et al. (1992) are shown. The [$m(152) - m(249)$] profile for M33 (Landsman et al. 1992) is similar but 0.6–0.7 mag bluer.

equal to that of the UV profiles, reflecting the associated origins of Hα and UV radiation in regions of recent star formation, although the individual sources do not correspond one-to-one at our resolution. In most cases, this is because the centroids of the H II regions imaged in Hα are not precisely coincident with the hot stars and reflection nebulae seen in the UV. Hα and UV photometry of individual sources in M74 are discussed in Cornett et al. (1994). The scale lengths of the optical-bandpass data agree with the results of Shostak & van der Kruit (1984), who give a value of 85″ for bandpasses approximating U, B, and V.

Figure 3 shows the results of the annular photometry displayed as radial profiles of the colors $m(152) - R$, $m(249) - R$, $B-R$, and $V-R$. These data confirm that M74's colors are bluer at larger radii in all colors measured relative to R and that this color gradient is larger for a larger wavelength difference; e.g., the $m(152) - R$ color gradient is larger in magnitude than the $m(249)-R$ gradient.

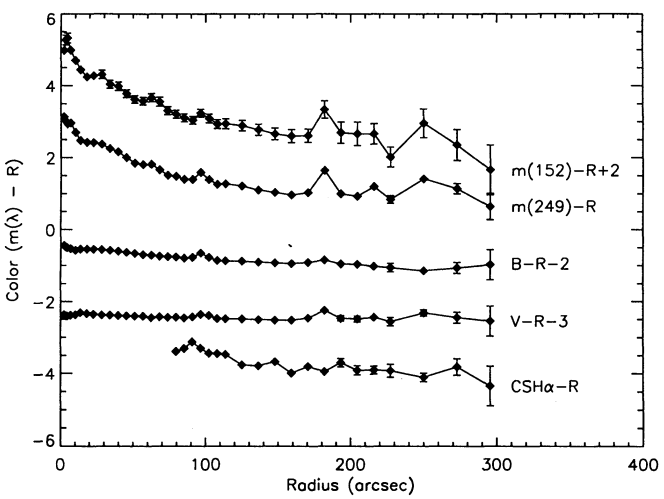

FIG. 3.—Radial color profiles for M74 for $m(152) - R$, $m(249) - R$, $B-R$, $V-R$, and CSHα $- R$. The 1 σ error bars are displayed where they are larger than plot symbols. Curves have been shifted vertically by the amounts noted. Color values for the CSHα $- R$ profile are uncertain for radii $\leq 75''$ because of uncertainties in continuum subtraction and are not plotted.

Figure 4 displays the $m(152) - m(249)$ UV color profile, with the colors of main sequence stars computed from an atlas of IUE stellar spectra (Fanelli et al 1992) displayed for reference. The color $m(152) - m(249)$ is near zero at the center, drops to $m(152) - m(249) \sim -0.2$ at $R = 10''$, and decreases to ~ -0.4 at $\sim 200''$ where the uncertain UV sky backgrounds begin to dominate. Details of the central $\sim 30''$ are discussed in § 3.3. The slope to the blue with radius is real at about the 2 σ level in the following sense: if we add 1 σ (from all sources) to the FUV sky and subtract 1 σ from the NUV sky, the slope of the plot for $20'' < R < 200''$ is no longer significantly different from zero. The observed $m(152) - m(249)$ color profile is much like that of M33 (Landsman et al. 1992), if the two galaxies are scaled to the same optical diameter, although M74 is about 0.5–0.6 mag redder. This difference in color is probably not due to foreground dust since M74's foreground reddening ($E[B-V] = 0.01$; see Turnrose 1975) is smaller than M33's (0.07; see van den Bergh 1991). We compare M74 and M33 further in § 4.

3.2. *Arms and Interarm Regions*

We investigate the photometric properties of arm and interarm regions separately by fitting a curve to the two principal spiral arms, which are clearly outlined in the UV. The arms are defined by selecting by eye the pixels in the part of the NUV image which are within the spiral arms; pixels in this region are then fitted by linear least squares with a logarithmic spiral. Figure 5 shows the UIT NUV image with the fit and tick marks, which define the arm and interarm patches, overlaid. Arm 1 and arm 2 (Hodge 1976) are labeled. The tick marks, which are 70 pixels (40″) long and 30 pixels (17″) apart, delineate the arm and interarm photometry regions as follows: rectangular "arm" patches of dimensions 70 pixels perpendicular to the arms as defined by the fit and 30 pixels (40″ × 17″) parallel to the arms, centered on the spiral, were used to define regions for the "arm" photometry. Rectangular patches 20

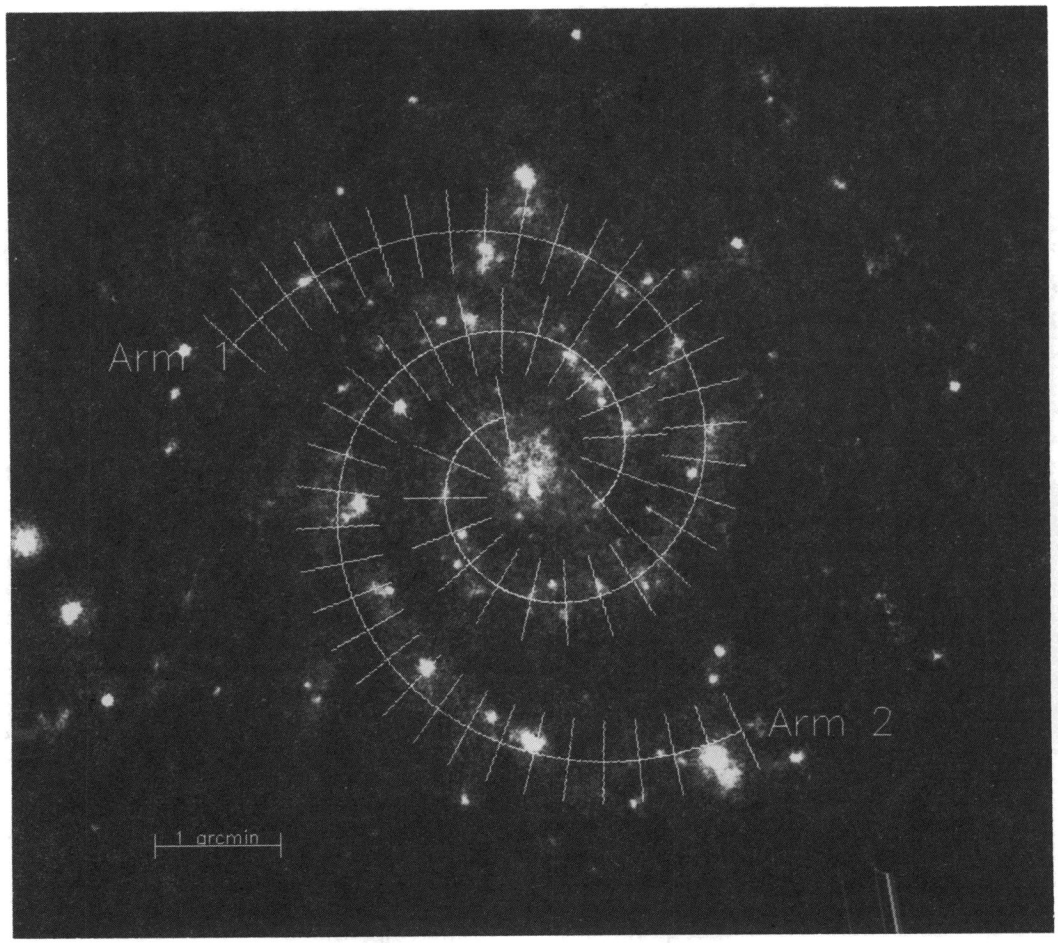

FIG. 5.—UIT NUV image of M74 with overlaid logarithmic spiral. The tick marks demonstrate the locations of arm and interarm patches. North is up and east is left; a 1′ bar, and arm 1 and arm 2 (Hodge 1976) are marked. The overlaid curve was produced by fitting an exponential spiral to eye-selected arm regions. Arm patches are defined as rectangles 70 pixels perpendicular to the arm by 30 pixels parallel to the arm (17″ × 40″) centered on the 70-pixel-long tick marks. Interarm patches are 20 pixels by 30 pixels (12″ × 17″) and are just inside and outside the arm patches at the ends of the tick marks.

pixels by 30 pixels (12″ × 17″) just inside and outside the "arm" patches were used to define the "interarm" photometry.

Figure 6 shows the results of [$m(152) - m(249)$] photometry in arm 1 (*diamonds*; *solid line*) and arm 2 (*circles; dashed line*) as a function of radius. The trend toward bluer colors with increasing radius is similar to that seen in the annular photometry plot (Fig. 4). The interarm profile is very noisy and is not shown. Red points [$m(152) - m(249) > 0$., e.g., at $\sim 80''$ and 130″ in arm 1] are generally associated with apertures which happen to contain no bright UV sources.

The arm-interarm photometry is consistent with the circular aperture photometry shown in Figure 4 for radii smaller than 160″. Uncertainties are large and difficult to estimate because they reflect the presence or absence of sources in particular apertures. The integrated mean interarm color for $R < 160''$ is [$m(152) - m(249)$] = -0.14 and the mean arm color is -0.31, while aperture photometry for that radial range gives -0.29. Therefore, the arms dominate the overall UV flux of M74, as expected from the appearance of the images. As in M33 (Landsman et al. 1992), interarm material is significantly redder in [$m(152) - m(249)$] than arm material.

3.3. *Nuclear Region*

The UV morphology of spiral galaxy nuclear regions varies considerably from "early" examples such as M31, which has a smooth UV nuclear bulge (Bohlin et al. 1985; O'Connell et al. 1992) to "late" examples such as M33, whose central region closely resembles spiral arm material in color and morphology (Landsman et al. 1992). Figure 1 shows that, in the UV, M74's nuclear region also has the overall morphological characteristics of spiral arm material: the nuclear region is patchy and noncircular, and there is no apparent nuclear bulge. Figure 7 is a plot of the annular-aperture [$m(152) - m(249)$] colors of the inner 20″ radius of M74. For this plot and color measurements of the nuclear region, a 4″ × 4″ region containing pixels affected by flux from a foreground star approximately 8″ south of the nucleus is masked out. In M74's nuclear region, significant color variations are confined to the central 10″ of radius and consist of a red peak of color [$m(152) - m(249)$] ~ 0.4 outside a core of color [$m(152) - m(249)$] ~ -0.2, which is approximately the color of much of the disk of M74. Outside the red peak, beyond a radius of about 9″, the profile flattens out at ~ -0.2.

Turnrose (1975) has computed a stellar synthesis model which reproduces optical scanner measurements of the central 10″ of M74. We have simulated the broad-band colors of his model by summing the UV fluxes of the component stellar types using an atlas of IUE stellar spectra (Fanelli et al. 1992). Turnrose's optimal model predicts a [$m(152) - m(249)$] color index of -0.92 mag. Our measured color index for M74 in a circular aperture of 10″ diameter is 0.1 ± 0.05. If this difference

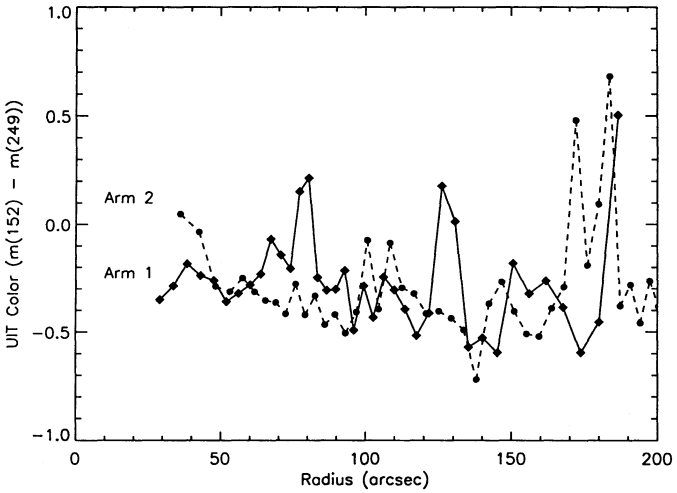

FIG. 6.—The [m(152) − m(249)] surface photometry in arm 1 (as defined by Hodge 1976; *diamonds and solid line*) and arm 2 (*circles and dashed line*) of M74, displayed as a function of radius. Photometry was performed in rectangular 70 × 30 pixel (40″ × 17″) apertures centered on the arms at the tick marks in Fig. 5. While there are large variations in the profile caused by the presence or absence of particular sources in apertures, the trend toward bluer colors with increasing radius is similar to that seen in the annular photometry plot of Fig. 4. Red points [m(152) − m(249) > 0., e.g., at ∼80″ and 130″ in arm 1] are generally associated with apertures which happen to contain no bright UV sources. The integrated mean interarm color for $R < 160''$ is [m(152) − m(249)] = −0.14, and the mean arm color is −0.31, while aperture photometry for that radial range gives −0.29.

in color is due to dust along the line of sight (a "screen"), it indicates a color excess $E(B-V)$ of 1.76 using the Galactic reddening curve of Savage & Mathis (1979), given E[m(152) − m(249)]/$E(B-V)$ = 0.58 for that curve. Only 0.01 of this color excess is accounted for by local Galactic dust (Turnrose 1975), while radio observations permit up to $E(B-V) = 0.33$, corresponding to a [m(152) − m(249)] reddening of 0.19, using dust-to-gas ratios of Bohlin, Savage, & Drake (1978). This discrepancy is probably explained by the lack of UV observational constraints in Turnrose's model. His optimal fits to M74 contain a small component of upper main sequence stars, but the scanner data are fit nearly equally well by a model which has no O or B stars. If we remove the O and B stars from his model, it predicts a color index [m(152) − m(249)] of −0.01, consistent with the UIT observations and moderate reddening. The UV observations therefore indicate that the central regions of M74 are not rich in OB stars, consistent with the lack of Hα emission (Pronik 1973). While star formation in the nuclear region has not been very active during the last ∼100 Myr, the UV-optical colors are consistent with significant star formation over the past few Gyrs (see § 4).

4. COLOR GRADIENTS IN M74 AND OTHER SPIRAL DISKS

4.1. *Abundance and Initial Mass Function Effects*

As is evident in Figures 3 and 4, M74 has a significant color gradient in its disk. In Figure 8, we show the UV/visual colors as a function of radius on an enlarged scale, where the [m(152) − V] color has been shifted down by 1 mag for clarity. Both colors change by ≥2 mag over the range plotted. The small difference in slope between the [m(152) − V] and [m(249) − V] colors accounts for the more modest change in m(152) − m(249) as a function of radius seen in Figure 4.

UIT has also been used to observe the spiral galaxies M33 (Landsman et al. 1992) and M81 (Hill et al. 1992; O'Connell et al. 1992). M33 is similar in its UV morphology to M74. UV-bright H II regions extend to the center of its disk. The H II regions are preferentially located in the spiral arms, though these are less organized and well defined than in M74. There is no evidence for a UV bulge in M33, whose bulge is also inconspicuous in optical bands but has been recently detected in the infrared by Minniti, Olszewski, & Rieke (1993). M81's UV image is quite different, with a smooth central bulge which is much smaller than at optical wavelengths. H II regions do not occur within $R \sim 5$ kpc of the nucleus. Outside this radius, H II regions are strongly concentrated to the most prominent spiral arms. The region of M81 near $R \sim 5$ kpc (outside the bulge but inside the innermost ring of H II regions) has an FUV flux < (2–3) × 10^{-19} ergs cm^{-2} Å^{-1} s^{-1}, which is too small to be measured reliably in the existing UIT images.

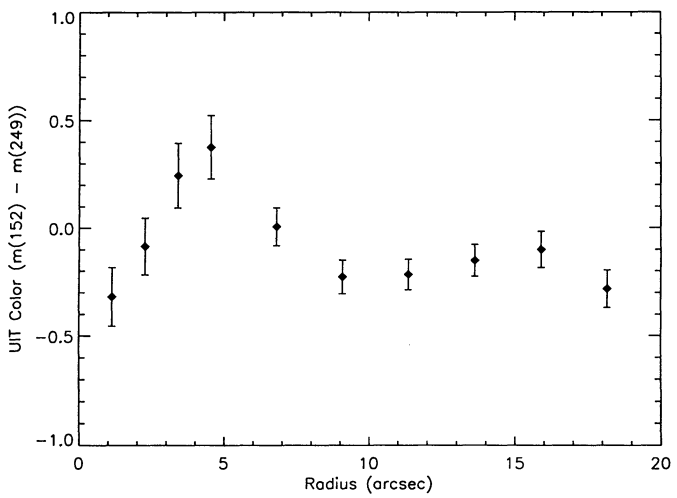

FIG. 7.—The [m(152) − m(249)] color profile of the nuclear region of M74 as measured in annular apertures. For this plot, a red foreground star 8″ south of the nucleus has been masked out. Note that the color flattens out at ∼ −0.2, the value for M74's disk (see Fig. 4) at a radius of about 9″.

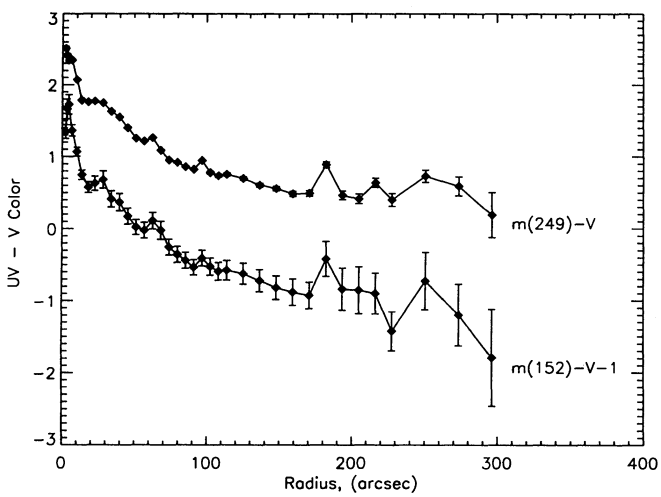

FIG. 8.—M74's m(249) − V and m(152) − V color profiles. The m(152) − V profile has been shifted down by 1 mag for clarity. No correction has been made to the observed profiles for foreground Galactic reddening, which amounts to [m(249) − V] = 0.04 and [m(152) − V] = 0.05.

TABLE 3

COMPARISON OF M33, M74, AND M81

Parameter	M33	M74	M81
General:			
Distance (Mpc)	0.72	7.2	3.2
Type	Scd	Sc	Sab
Optical colors:			
$B-V$ (total)	0.55	0.64	0.95
$U-B$ (total)	−0.10	0.01	...
$m(152)-m(249)$ colors:			
Nuclear region	−0.6 ($R < 2'$)	0.1 ($R < 10''$)	0.8 ($R < 20''$)
Inner disk	−0.7	−0.2	0.0 ($R > 200''$)
Outer disk	−0.9	−0.4	0.0
[O/H] Abundance gradient fits:			
Slope (dex kpc^{-1})	−0.09 ± 0.03	−0.081 ± 0.002	−0.080 ± 0.035
Central value	8.82	9.20	9.36

Table 3 lists mean $m(152)-m(249)$ colors and other information for the nuclear regions and the inner and outer disks of the three galaxies. Aperture sizes for the "nuclear region" measurements have been scaled to include approximately $R < 400$ pc at the adopted distances. Distances are from Belley & Roy (1992), and other data are from de Vaucouleurs et al. (1991). Abundance information is based on compilations of oxygen abundance measurements in H II regions by Belley & Roy (1992) and Vila-Costas & Edmunds (1992). M74 and M81 have central oxygen abundances approximately equal to that of the Galaxy; M33 has a significantly smaller central oxygen abundance by 0.3–0.5 dex. The slopes of the abundance gradients in units of dex kpc^{-1} are equal within uncertainties for the three galaxies. However, the mean oxygen abundances of the disk regions with UV measures (corresponding to roughly one disk scale length) differ significantly, being 8.98, 8.70, and 8.66, respectively, for M81, M74, and M33.

Table 3 shows that M74 is intermediate between M33 and M81 in overall UV color and in nuclear-region/disk color difference. M33's nuclear region is essentially the same color in $m(152)-m(249)$ as its disk; M81 has a much redder bulge, and M74 is between the two. The disks of both M33 and M74 show significant color gradients in $m(152)-m(249)$, with the outer regions being bluer, whereas M81's disk appears to be more uniform, except at small radii.

The color differences between these galaxies and the gradients within their disks could be explained by reddening due to internal dust, stellar abundance variations, initial mass function (IMF) variations, the history of formation of the dominant generations of stars, or a combination of these. We consider stellar abundances first. An abundance difference in the stellar populations would be expected from the mean gas phase abundances in the three objects (Table 3) and from their observed outward decline. The UV energy distributions of hot stars are affected by metallic line blanketing (Kurucz 1992). Decreasing metallicity will make the UV colors bluer, other things remaining constant, which is in the correct sense to explain both the difference in mean UV colors between the galaxies and the measured color gradients.

We have used the Landsman (unpublished; described in Hill et al. 1993) evolutionary synthesis models, described below, to estimate the dependence of UV color on abundance as a function of stellar population age. We find that for ages near 200 Myr, approximately corresponding to the mean UV colors of the disks, that $\partial[m(152)-m(249)]/\partial Z \sim 0.25$ mag dex^{-1}. This value is uncertain owing to incomplete line lists for modeling UV line blanketing in stellar atmospheres. Nonetheless, it is considerably smaller than the value of ~ 2 mag dex^{-1} which would be necessary to explain all of the difference in the mean disk colors of M33, M74, and M81 by abundance differences alone. This explanation of the colors would also have required an unreasonable synchronization in star formation between these three separate systems. Furthermore, the large gradients in UV-optical color seen in M74's disk (Fig. 8) are over 4 times larger than would be expected from the gradient in gas phase abundances. Stellar abundance variations alone therefore do not appear to be responsible for the large-scale color effects seen in these disks. A similar conclusion was reached for M33 by Landsman et al. (1992).

Similarly, variations in the IMF cannot explain the amplitude of the observed effects. A change in the IMF power law index from −1 to −2 does not change the predicted $[m(152)-V]$ or $[m(249)-V]$ colors by more than ~ 0.1 mag at an age of 200 Myr.

4.2. *Star Formation History and Extinction Effects*

To examine the effects of star formation history and internal reddening, we use a UV two-color diagram (Fig. 9*a*), similar to the more familiar $(U-B)$, $(B-V)$ versions used at optical wavelengths (e.g., Searle, Sargent, & Bagnuolo 1973; Larson & Tinsley 1978). The UV colors for various fiducial stellar populations in this diagram have been derived from three sets of evolutionary synthesis models: Bruzual & Charlot (1993), Landsman (unpublished), and our own. The colors of Bruzual and Charlot are based mainly on the evolutionary tracks of Maeder & Meynet (1989) and on the Heck et al. (1984) and Wu et al. (1991) compilations of *IUE* UV spectra. The Landsman colors employ the more recent evolutionary tracks of Schaller et al. (1992) and the theoretical model atmospheres of Kurucz (1992). Our set of models is based on the semiempirical populations derived mainly from cluster color-magnitude diagrams by O'Connell (1983) and the library of *IUE* spectra compiled by Fanelli et al. (1992). From each of the three sets of models we obtained the UV spectral energy distributions predicted for single-generation populations covering a range of ages from 5 to 10,000 Myr, assuming solar metal abundances and a Salpeter IMF. The broad-band colors were then derived using the measured UIT filter/detector response curves. We have omitted from the colors the effects of horizontal-branch (HB) and post-HB hot populations in older models ($t > 5000$ Myr);

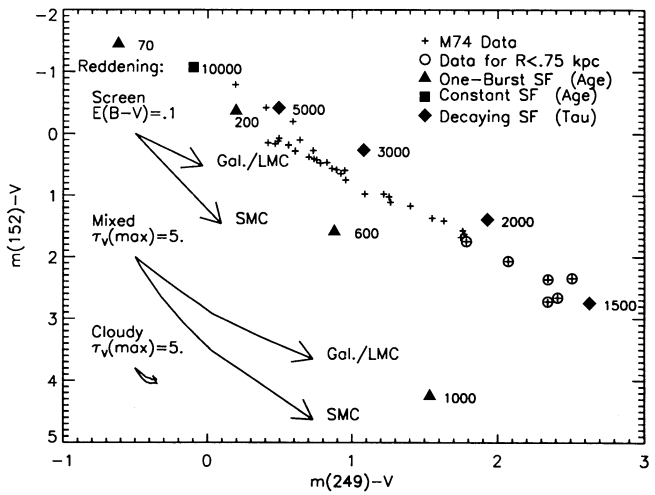

FIG. 9a

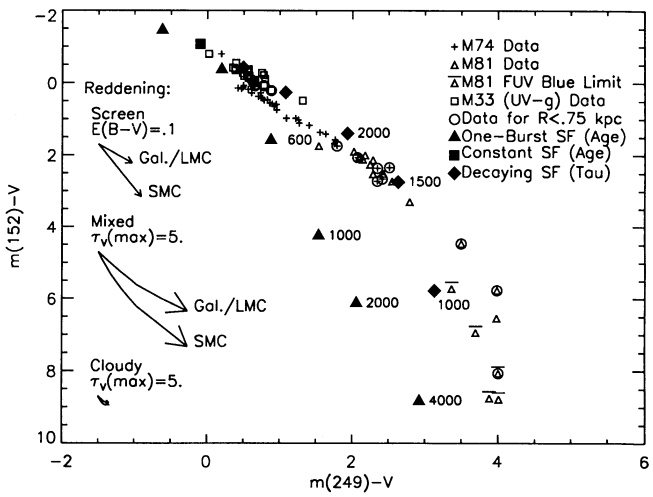

FIG. 9b

FIG. 9.—(*a*) The $[m(249) - V]$ vs. $[m(152) - V]$ colors of M74 as observed (*plus signs*). The reddest colors, e.g., $m(249) - V > 1.7$, are from $R < 20''$ and are circled. Filled triangles represent single-burst star-formation models of ages 70, 200, 600, and 1000 Myr (with ages marked); the filled square represents a continuous constant-rate star-formation model of age 10,000 Myr; and diamonds represent 10,000 Myr continuous star-formation models with star formation which decays with timescales of 5000, 3000, 2000, and 1500 Myr (with timescales marked). Also shown are reddening trajectories computed using interstellar reddening curves for our Galaxy (Savage & Mathis 1979) and the Small Magellanic Cloud (Hutchings 1982) for three different assumed models. The "screen" model assumes all dust to be between the stars and the observer, has maximum $E(B-V) = 0.1$, and includes only absorption by dust. The "mixed" model uses the results of Witt et al. (1992) for a "dusty" galaxy, which assumes stars are in a dust-free sphere surrounded by a spherical star-free shell of dust. The "cloudy" model, also after Witt et al. (1992), assumes the dust to be in a uniform small sphere contained within a larger uniform sphere of stars. The "mixed" and "cloudy" models are parameterized by the total optical depth in the V band and τ_V which has maximum value 5, corresponding to $E(B-V) = 1.75$ for the "screen" model. (*b*) The $[m(249) - V]$ vs. $[m(152) - V]$ colors as in (*a*) but including data from UIT and ground-based observations of M33 (*open squares*) and M81 (*open triangles*). The reddest colors, from the central 1.5 kpc radius of the galaxies are circled. Triangles with bars are $[m(152) - V]$ blue limits in the low-FUV-flux region of M81 ($50'' < R < 200''$). This figure extends to redder (UV − V) values in both axes than (*a*). M33 data are (UV − G) values. The three galaxies occupy a continuum, with M33 bluest, M81 reddest, and M74 between.

this is not important to the discussion here but does affect the colors as plotted in Figure 9. There is significant scatter in the predictions at a given age, reflecting different assumptions in the modeling. Rather than attempting to choose between them, we have simply averaged the results from the three sets.

The colors for single generations, together with the corresponding M/L ratios, have then been combined to compute the colors of a 10,000 Myr–old system with a constant star-formation rate and the colors of 10,000 Myr–old systems with exponentially declining star-formation rates and e-folding times of 1500, 2000, 3000, 5000, and 10,000 Myr. The results are shown in Figure 9*a*. The colors of other combinations of the single generation models can be inferred from the figure, though the pairwise combination lines are curved in this logarithmic diagram.

The M74 annular aperture photometry is also plotted in Figure 9*a* as plus signs. Measures in the nuclear region ($r < 20''$, circled), are the reddest in the galaxy. These fall near the location of unreddened exponentially declining models with e-folding times of 1500–2000 Myr. Measures at larger radii extend blueward in a straight line from this region to the vicinity of the unreddened 200 Myr–old single generation model. With the exception of a couple of low-precision measurements, all of the data points fall considerably to the red of the constant star-formation model. Most of the data are also slightly redder in $[m(152) - V]$ than the locus of exponentially declining star-forming models.

Several conclusions can immediately be drawn from the locus of the observations. First, all of the disk, including the region at $R < 20''$, has experienced significant star formation during the past 500 Myr. The star-formation history or the extinction also clearly varies considerably from place to place in the disk. The location corresponding to unreddened H II regions, i.e., single generations with ages >5 Myr, falls off the plots in Figure 9*a* at $(-2.18, -3.45)$. This is well to the blue of any of the measured M74 colors, implying that unreddened H II regions do not make a major contribution to the total UV light.

We have obtained photometry of the resolved H II regions, to be presented in a later paper (Cornett et al. 1994), and find that these contribute only about 29% of the 1520 Å and 27% of the 2490 Å integrated light. Although these values are preliminary, it appears that the UV light in M74 is dominated by the diffuse component. A similar computation of the relative contributions of diffuse and resolved structure in M33 at 2000 Å by Buat et al. (1993) found that at least 50% of the 2000 Å integrated light is contributed by sources (86% after correction for dust extinction).

Figure 9*a* also shows reddening trajectories generated using the interstellar extinction laws for our Galaxy (Savage & Mathis 1979) and the Small Magellanic Cloud (SMC) (Hutchings 1982). (On the scale of the diagram, results derived using the LMC reddening law of Fitzpatrick 1985 are nearly coincident with those using Galactic reddening and are not illustrated.) It is clear that the geometry of the star/dust mixture has a controlling influence on the reddening and that this will be of special importance in the UV (Witt et al. 1992 and references therein). Three different extinction trajectories are shown in the figure. The "screen" model assumes that all dust lies between the source and the observer and ignores emergent scattered photons. The upper pair of vectors shows Galactic and SMC screen reddening for the moderate value of $E(B-V) = 0.1$. The screen geometry establishes an upper limit to the effects of dust on the colors, as discussed by Witt et al.

(1992). The screen model is unlikely to be realistic for most spiral galaxies (e.g., Bruzual, Magris, & Calvet 1988; Disney, Davies, & Phillips 1989; Witt, Thronson, & Capuano 1992), although the presence in M74 of a warped disk associated with the possible infall of a companion galaxy may signal a disturbed dust layer which might produce screenlike effects (Kamphius & Briggs 1991).

Other star/dust geometries will produce smaller effects on the colors for a given amount of dust. In Figure 9*a* we also plot two more realistic models based on the calculations of Witt et al. (1992), which include the effects of scattering in a spherical geometry. Their "UVB" and "UVA" cases correspond approximately to our 1520 Å and 2490 Å bands, respectively. The "mixed" trajectory is for a uniform sphere of stars and dust (called a "dusty galaxy" model by Witt et al.) and is parametrized by the optical depth of the dust in the V band, τ_V, which increases from 0 to 5 in this plot [corresponding to $E(B-V) = 0$ to 1.75 for a screen model]. Such a geometry might apply to stars recently born in the central interstellar medium (ISM) layer of a spiral galaxy. This model results in reddening behavior similar to the screen but with much smaller effective reddening per unit dust mass [e.g., a factor of ~ 6.6 in $m(249) - V$ for the Galactic reddening curve at $\tau_V = 5$.] For large optical depths, the color of the emergent radiation approaches an asymptotic value. The third model, denoted "cloudy" by Witt et al., corresponds to a system where the dust is confined to a smaller sphere inside a homogeneous sphere of stars. This model might apply to an intermediate age region of a spiral disk, where the stars have diffused outside the dust layer. The cloudy model produces relatively little reddening, with maximum effects approximately equal to screen models with $E(B-V) \sim 0.02$ at $\tau_V \sim 2$, but decreasing effects for larger τ_V.

The various reddening trajectories in Figure 9 roughly parallel the age trajectories for single generations younger than ~ 600 Myr or models with e-folding times longer than 1500 Myr. This means that it is difficult, without further information, to unambiguously distinguish age from reddening effects. For example, the well-defined locus of colors for the M74 disk could be interpreted as a population with a single age of ~ 200 Myr on which is imposed screen reddening ranging from $E(B-V) \sim 0.05$ in the outer disk to ~ 0.5 in the nucleus. Such a model might apply to a starburst system with a unique and brief period of star formation but is unlikely to be realistic for a galaxy like M74 with well-developed spiral structure and H II regions. Alternatively, M74's disk could be interpreted as having a well-defined relationship between e-folding time and radius, ranging from a time of ~ 5000 Myr in the outer disk to ~ 2000 Myr in the nucleus, coupled with modest screen or mixed reddening with an SMC-type extinction law.

However, we do have some additional information to place constraints on reddening and star-formation history. For the nucleus, Turnrose's (1975) optical spectrophotometry and synthesis modeling indicates only modest reddening, $E(B-V) \sim 0.10$, which in Figure 9*a* would imply an exponentially declining model with an e-folding time of ~ 2000 Myr for the inner 20″ of the disk, which is consistent with Turnrose's own tests of such models.

There is also good radio evidence on the distribution of the interstellar medium within M74. We have summed column density profiles for H I (Shostak & van der Kruit 1984) and H_2 (from CO observations of Adler & Liszt 1989) to derive a predicted $E(B-V)$ profile from the gas-to-dust ratio of Bohlin, Savage, & Drake (1978) [$N(\mathrm{H\ I} + \mathrm{H_2}) = 5.8 \times 10^{21}\ \mathrm{cm}^{-2}/E(B-V)$]. [Assuming one-half the total gas column density to be on the near side of M74, we have divided the observed column densities by 2 to compute $E(B-V)$]. The radio observations predict $E(B-V)$ values in the screen geometry ranging from 0.33 over the central 30″ radius to 0.07 at the edge of the optical disk. More metal-poor regions at larger radii would likely have a smaller ratio of dust to H I, which would exaggerate the radial gradient in extinction. However, the fact that the radio data predict a central reddening in the screen model higher than obtained by Turnrose suggests that the screen geometry is inappropriate there. If the "mixed" or "cloudy" geometries are also more realistic for the rest of the disk of M74, then it appears that most of the range of (UV − V) color in Figure 9*a* results from changes in the star-formation history rather than in the extinction.

4.3. *Comparison to M33 and M81*

Figure 9*b* is similar to Figure 9*a* but includes data from UIT and ground-based observations of M33 (*open squares*; Landsman et al. 1992) and M81 (*open triangles*; Hill et al. 1992) and extends to redder (UV − V) values in both axes. The M81 data have been smoothed and binned to 0.5 intervals. Open triangles with bars are [$m(152) - V$] blue limits for the inner disk region of M81 ($50'' < R < 200''$), which has very low FUV flux. The M33 points use G-band rather than V-band data, but corrections would be very small on the scale of this plot. For all three galaxies, measurements of the central ~ 1.5 kpc diameter are denoted by circled symbols.

The three galaxies occupy a continuum, with M33 bluest, M81 reddest, and M74 lying between. The small range of colors occupied by M33 reinforces the conclusions of Landsman et al. that M33 has no UV bulge population and that its color variations could be explained by the effects of dust extinction. The outer regions of the M74 disk overlap the colors of much of M33's disk. The small vertical displacement of ~ 0.5 in $m(152) - V$ color between M33 and M74 may be due to abundance effects, since it is similar to color differences in Figure 9*b* computed for stellar atmospheres (Kurucz 1992) of similar (UV − V) colors which have the abundances observed in the two galaxies (see Table 3). M81 clearly contains a range of stellar populations. Its bulge is quite red, though it contains a contribution from the UV excess (UVX) component, presumably low-mass stars on the hot horizontal branch and subsequent evolutionary phases (O'Connell et al. 1992). The bluest regions of M81's disk overlap the (reddest) inner regions of the M74 disk.

M74's disk therefore contains material which spans the (UV − V) colors characteristic of M33 and the more active star forming regions of M81. All material in this color range in all three galaxies has the morphological appearance of disk/spiral arm material. If, as seems likely, extinction from dust can contribute only modest effects on the scale of Figure 9*b*, then most of the color range observed results from differences in the star-formation history between and within the three objects. A combined program of UV, optical, and radio observations could readily improve constraints on these histories.

5. SUMMARY

UIT and ground-based optical photometry define surface brightness and color profiles for M74. All surface brightness profiles have a central peak and approximately exponential falloff; the scale lengths of the falloff increase with decreasing

wavelength, and the continuum-subtracted Hα profile has a scale length between the NUV and FUV values. Each of M74's color profiles becomes bluer with increasing radius. The $[m(152) - m(249)]$ color is near 0.0 in the central 20″ radius and decreases from ~ -0.2 to ~ -0.4 between 20″ and 200″ radius. Photometry in the spiral arms gives similar results, with interarm regions slightly redder. M74's nuclear region has the appearance of disk material in the UV. UIT colors for the central 10″ region demonstrate that there are no O or B stars present, consistent with the lack of Hα emission.

We have compared M74's UV colors with those of M33 and M81. M74's UV morphology and $[m(152) - m(249)]$ color profiles are similar to those of M33, although M74 is ~ 0.5 mag redder. M81 has a smooth UV bulge, which is much redder than M74 and M33's nuclear regions, and has H II regions only in spiral arms > 5 kpc from its center. M74 is ~ 0.4 mag bluer than M81 in its outer disk. Abundance and IMF variations do not produce large enough $m(152) - m(249)$ or $UV - V$ color differences to account for M74's range of colors or the differences among the galaxies.

Comparing UV/optical model colors with those of M74 shows that M74's disk has undergone significant star formation over the past 500 Myr and that either the star-formation history or the extinction varies systematically across M74's disk. Realistic reddening models show that the effects of dust alone are not sufficient to reproduce the variations within M74. However, evolutionary models produced by combining data from stellar atmospheres and observed spectra generate $UV - V$ colors which are compatible with the observations, provided relatively recent star formation has occurred.

M74 colors range from the bluest of M33's colors to the bluest of M81's. All material with these colors in all three galaxies has the appearance of spiral arm/disk material. The failure of reddening models to cover the range of colors, and the known abundance range in such material, imply that star-formation history varies significantly as a function of radius in these galaxies and that such variation is necessary to explain the range of colors observed in M74, M33, and M81.

Many people contributed to the success of the Astro-1 mission and the UIT experiment, and we gratefully acknowledge them collectively here. We thank Mike Fanelli, Jesse Hill, and Wayne Landsman for useful discussions. Funding for the UIT project has been through the Spacelab Office at NASA Headquarters under Project number 440-51. R. W. O. acknowledges NASA support of portions of this research through grants NAG 5-700 and NAGW-2596 to the University of Virginia.

REFERENCES

Adlers, D. S., & Liszt, H. S. 1989, ApJ, 339, 836
Belley, J., & Roy, J.-R. 1992, ApJS, 78, 61
Bohlin, R. C., Cornett, R. H., Hill, J. K., Hill, R. S., O'Connell, R. W., & Stecher, T. P. 1985, ApJ, 298, L37
Bohlin, R. C., Savage, B. D., Drake, J. F. 1978, ApJ, 224, 132
Bruzual A, G., & Charlot, S. 1993, ApJ, 405, 538
Bruzual A, G., Magris, G., & Calvet, N. 1988, ApJ, 333, 633
Buat, V., Vuillemin, A., Burgarella, D., Milliard, B., & Donas, J. 1993, A&A, in press
Chen, P. C., et al. 1992, ApJ, 395, L41
Cornett, R. H., et al. 1994, in preparation
de Vaucouleurs, G., de Vaucouleurs, A., Corwin, H. G., Jr., Buta, R. J., Patuel, G., & Forque, P. 1991, 3d Reference Catalogue of Bright Galaxies (New York: Springer-Verlag)
de Vaucouleurs, G., de Vaucouleurs, A., & Corwin, H. G., Jr. 1978, AJ, 183, 1331
Disney, M., Davies, J. I., & Phillipps, S. 1989, MNRAS, 239, 939
Fanelli, M. N., O'Connell, R. W., Burstein, D., & Wu, C.-C. 1992, ApJS, 82, 197
Fitzpatrick, E. L. 1985, ApJ, 299, 219
Heck, A., Egret, D., Jaschek, M., & Jaschek, C. 1984, *IUE* Low-Dispersion Reference Atlas (Noordwijk: ESA)
Hill, J. K., Bohlin, R. C., Cheng, K.-P., Hintzen, P. M. N., Landsman, W. B., Neff, S. G., O'Connell, R. W., Smith, A. M., Smith, E. P., & Stecher, T. P. 1992, ApJ, 395, L37
Hill, J. K., Isensee, J. E., Bohlin, R. C., O'Connell, R. W., Smith, A. M., & Stecher, T. P. 1993, ApJ, 414, L9
Hodge, P. W. 1976, ApJ, 205, 728
Hutchings, J. B. 1982, ApJ, 255, 70
Kamphius, J., & Briggs, F. 1991, in Warped Disks and Inclined Rings around Galaxies, ed. S. Casertano, P. Sackett, & F. Briggs (Cambridge: Cambridge Univ. Press), 190
Kennicutt, R. C., & Hodge, P. W. 1980, ApJ, 241, 573
Kurucz, R. L. 1992, in The Stellar Populations of Galaxies, ed. B. Barbuy & A. Renzini (Dordrecht: Kluwer) 225
Landsman, W. B., Roberts, M. S., Bohlin, R. C., O'Connell, R. W., Smith, A. M., & Stecher, T. P. 1992, ApJ, 401, L83
Larsen, R. B., & Tinsley, B. M. 1978, ApJ, 221, 554
Maeder, A., & Meynet, G. 1989 A&AS, 76, 411
Minniti, D., Olszewski, E., & Rieke, M. 1993, ApJ, 410, L79
O'Connell, R. W. 1983, ApJ, 267, 80
O'Connell, R. W., Bohlin, R. C., Collins, N. R., Cornett, R. H., Hill, J. K., Hill, R. S., Landsman, W. B., Roberts, M. S., Smith, A. M., & Stecher, T. P. 1992, ApJ, 395, L45
Pronik, I. I. 1973, AZh, 16, 628
Savage, B. D., & Mathis, J. S. 1979, ARA&A, 17, 73
Schaller, G., Schaerer, D., Meynet, G., & Maeder, A. 1992, A&AS, 96, 269
Searle, L., Sargent, W. L. W., & Bagnuolo, W. G. 1973, ApJ, 179, 427
Shostak, G. S., & van der Kruit, P. C. 1984, A&A, 132, 20
Stecher, T. P., et al. 1992, ApJ, 395, L1
Turnrose, B. 1975, ApJ, 210, 33
van den Bergh, S. 1991, PASP, 103, 609
Vila-Costas, M. B., & Edmunds, M. G. 1992, MNRAS, 259, 121
Witt, A. W., Thronson, H. A., & Capuano, J. M., Jr. 1992, ApJ, 393, 611
Wu, C.-C., Crenshaw, D., Blackwell, J. H., Wilson-Diaz, D., Schiffer, F. H., Burstein, D., Fanelli, M. N., & O'Connell, R. W. 1991, The *IUE* Ultraviolet Spectral Atlas Addendum I (Greenbelt: NASA/GSFC)